

The Frequency Shift and Q of Disordered Superconducting RF Cavities

Hikaru Ueki,^{1,2,*} Mehdi Zarea,^{1,2,†} and J. A. Sauls^{1,2,‡}

¹*Hearne Institute of Theoretical Physics, Louisiana State University*

²*Center for Applied Physics & Superconducting Technologies,
Northwestern University & Fermi National Accelerator Laboratory*

(Dated: December 13, 2024)

Niobium superconducting radio-frequency (SRF) cavities for high energy accelerator applications have been greatly improved in terms of the quality factor Q by techniques such as Nitrogen doping. However, the mechanisms leading improvement in Q are still not fully understood. Quite recently the SRF group at Fermilab measured anomalies in the frequency shift of N-doped SRF Niobium cavities near the transition temperature. Here we report our theoretical analysis of these results based on the microscopic theory of superconductivity that incorporates anisotropy of the superconducting gap and inhomogeneous disorder in the screening region of the SRF cavities. We are able to account for frequency shift anomalies very close to T_c of the order of fractions of a kHz. Our results for the frequency shift and Q are in good agreement with the experimental data reported for all four N-doped Nb SRF cavities by Bafia et al. We also compare our theory with an earlier report of on a Nb sample measured at 60 GHz. In addition we show that the quality factor calculated theoretically has a peak of upper convexity with the largest Q at intermediate levels of disorder. For strong disorder, i.e. the dirty limit, pair breaking in the presence of disorder and screening currents limits the Q .

I. INTRODUCTION

The performance of Niobium-based superconducting radio-frequency (SRF) cavities, as measured by the quality factor Q and superheating field, H_s , for high energy physics accelerator technology have been improved significantly by techniques such as Nitrogen infusion [1]. High- Q SRF cavities are also being proposed and developed as detectors in the search for dark matter candidates. In recent proposals the sensitivity of the SRF cavity to axion-like dark matter detection depends on the square of the quality factor [2, 3]. SRF cavities operating at ultra-low temperatures and minimal microwave power have also attracted attention for applications in quantum information technology [4].

However, doping and impurity infusion mechanisms leading to improved performance are not fully understood. The roles of disorder and inhomogeneity on the current response near the vacuum-superconducting interface can lead to both subtle and competing effects [5, 6]. Given the range of applications of high- Q SRF cavities a more detailed understanding of the effects of disorder on SRF performance is called for that combines first-principles theory of superconductivity, materials analysis and characterization. Recent measurements of the resonant frequency of Nb-based SRF cavities with different surface treatments reveal non-monotonic temperature dependence (“anomalies”) in the shift of the resonant frequency of the cavity just below the superconducting transition, $\delta f = f_s(T) - f_n(T_c)$, for $|T - T_c| \ll T_c$. These anomalies are sensitive to surface treatment [7]. For Nitrogen-doped Nb SRF cavities these authors observed a negative slope in the resonance frequency just below the transition temperature, a minimum negative shift and rapid increase over a narrow temperature range just below T_c [7]. Anomalies in the frequency shift just below T_c for Nb coupled to a tunnel-diode oscillator operating at 10 MHz were reported much earlier [8, 9]. Similar analysis of the impedance data of a Niobium sample embedded in a cylindrical copper cavity [10] implies an anomaly in the resonance frequency shift at a nominal frequency of 60 GHz [11]. The results for the frequency shift and Q reported

by Bafia et al. for N-doped Nb SRF cavities cover the frequency range 0.65 – 3.9 GHz [7].

We report results based on the microscopic theory of nonequilibrium superconductivity [12–14], combined with Slater’s method for solving Maxwell’s equations for the EM field confined in a closed metallic cavity [15], for the frequency shift, δf , and quality factor Q of the cavity as functions of temperature, frequency and disorder. We are able to calculate frequency shifts of order $\delta f \sim 1 - 10^3$ Hz that exhibit non-monotonic behavior over a narrow temperature range, $|\Delta T|/T_c \lesssim 10^{-3}$, that are sensitive to impurity disorder. Indeed analysis of the frequency shift data near T_c can provide a powerful method for measuring the scattering rate of electronic excitations by the random disorder potential. In addition, the dependence of Q as a function of the scattering rate from the random potential is calculated and shown to exhibit a peak of upper convexity with a maximum Q obtained for cavities with intermediate levels of disorder, $1/2\pi\tau T_c \sim 1$. For strong disorder, $1/2\pi\tau T_c \gg 1$, pair breaking strongly suppresses Q [16]. These results are discussed in Sec. IV.

Our theoretical predictions and analysis of δf and Q in the weak coupling limit for superconductors with disorder is in good agreement with experimental data reported for N-doped Niobium SRF cavities. An important element of the theory is the impact of disorder on the suppression of T_c resulting from pair-breaking induced by the interplay of gap anisotropy and impurity scattering, i.e. weak violation of Anderson’s theorem by non-magnetic disorder [17]. Inhomogeneous disorder then generates an inhomogeneous distribution for T_c distributed throughout an SRF cavity. These results and comparison with experimental results on N-doped Nb cavities are reported in Sec. IV C.

We begin with the theoretical formulation and theoretical results for the a.c. conductivity of disordered superconductors, then connect the a.c. conductivity to the complex surface impedance in Sec. II. The key results of Slater’s method connecting the surface impedance to the resonance frequency shift, δf and Q of the cavity are discussed in Sec. III. The more technical aspects of the theoretical formalism are discussed in Appendix A. We use the the formalism of Ref. 14 for the a.c. conductivity in superconductors based on the quasiclassical theory of superconductivity. We incorporate gap anisotropy and inhomogeneous disorder to calculate the conductivity for superconducting RF cavities. We employ Slater’s formulation for solving Maxwell’s

* uekih@lsu.edu

† zarea.mehdi@gmail.com

‡ sauls@lsu.edu

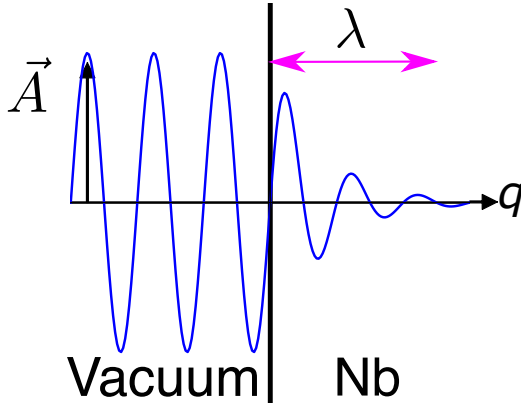


FIG. 1. Transverse electromagnetic field penetration represented by the vector potential at a vacuum-superconductor interface. In the superconducting state field penetrations a distance of order the London penetration depth, λ , while in the normal state field penetration is governed by the skin depth, $\delta(\omega) = c/\sqrt{2\pi\omega\sigma_n}$, where σ_n is the normal-state conductivity at frequency ω .

equations [15, 18] and derive relations between the conductivity and surface impedance in superconductors in the local limit, as well as expressions for the frequency shift and quality factor in Sec. III. We also derive the frequency shift near T_c and show that the frequency shift has various types of anomalies near T_c that are sensitive to the level of disorder. In Sec. IV we compare our calculations of the frequency shift and quality factor with the two experimental results of Klein et al. [10, 11] and Bafia et al. [7].

II. CURRENT RESPONSE OF AN RF CAVITY

Consider the current response and penetration of the electromagnetic field at the vacuum-metal interface of an SRF cavity as illustrated in Fig. I. In this geometry the electric and magnetic fields are transverse to the interface normal, and the corresponding surface current for an isotropic superconductor takes the form, $\mathbf{J}(\mathbf{q}, \omega) = K(\mathbf{q}, \omega) \mathbf{A}(\mathbf{q}, \omega)$, where $K(\mathbf{q}, \omega)$ is the linear response function determining the Fourier components of the current in terms of those of the EM field; $K(\mathbf{q}, \omega)$ encodes the response of unbound quasiparticles, as well as the response of superconducting condensate, to the EM field and the random potential.

Pure Niobium is a superconductor that is near the border between type I and type II magnetic behavior, i.e. with a London penetration depth, λ , comparable to the superconducting coherence length, ξ [19]. However, disorder increases the London penetration depth and also reduces

the coherence length, driving Nb with disorder to type II behavior. In this limit the electromagnetic field penetrates relatively deep into the superconductor at a vacuum/superconducting interface and probes the *bulk* order parameter by exciting currents relatively far from the interface. Thus, we neglect the surface deformation of the order parameter on the scale of ξ and calculate the current response to the EM field in the local limit, in which case we can set $q = 0$ in the response function, $K(\mathbf{q}, \omega)$. The current response then reduces to

$$\mathbf{J}(\mathbf{q}, \omega) = \sigma(\omega) \mathbf{E}(\mathbf{q}, \omega), \quad (1)$$

where $\sigma(\omega) \equiv -icK(0, \omega)/\omega$ is the a.c. conductivity. To calculate $K(\mathbf{q}, \omega)$, and thus $\sigma(\omega)$, we solve the non-equilibrium quasiclassical transport equations, originally formulated by Larkin and Ovchinnikov and Eliashberg [12, 13]. Here we use the Keldysh formulation of nonequilibrium quasiclassical transport theory for strong-coupling and disordered superconductors in Ref. 14. The current response is then given in terms of the τ_3 -component of the Keldysh propagator,

$$\mathbf{J}(\mathbf{q}, \omega) = N_f \int d\mathbf{p} (e\mathbf{v}_p) \int_{-\infty}^{\infty} d\epsilon \frac{1}{2} \text{Tr} \{ \hat{\tau}_3 \hat{\mathcal{G}}^K(\mathbf{p}, \mathbf{q}; \epsilon, \omega) \}, \quad (2)$$

where $\hat{\mathcal{G}}^K(\mathbf{p}, \mathbf{q}; \epsilon, \omega)$ is the solution of the Keldysh transport equations for the Keldysh component of the nonequilibrium propagator. Note that N_f is the total normal-state density of states at the Fermi energy, $e\mathbf{v}_p$ is current carried by normal-state quasiparticles with Fermi velocity, \mathbf{v}_p , for the point \mathbf{p} on the Fermi surface, and e is the electron charge. Pairing correlations and particle-hole coherence of the Bogoliubov excitations of the superconducting state are encoded in the Nambu structure of $\hat{\mathcal{G}}^K$, the pairing self energy, Δ , and the Nambu matrix structure of the transport equations.

Here we consider the response of a conventional isotropic superconductor in the long-wavelength limit ($q \rightarrow 0$) with disorder in the form of a random distribution of non-magnetic impurities. In the normal state the random potential leads to diffusive transport described by a mean transport scattering time, τ , or mean free path, $\ell = v_f \tau$, where v_f is the Fermi velocity for an isotropic metal. Electron-phonon retardation effects are relatively small for Nb, with corrections to the gap of order a few percent [17]. Thus for the purposes of calculating the current response we evaluate the equilibrium pairing self energy in the weak-coupling limit, $T_c \ll \omega_D$. With these assumptions the current response function for a conventional superconductor given by Eq. (68) of Ref. [14] reduces to

$$\begin{aligned} \sigma(\omega) = & \frac{\sigma_D}{i\omega\tau} \int_{-\infty}^{\infty} \frac{d\epsilon}{4\pi i} \left\{ \tanh\left(\frac{\epsilon - \omega/2}{2T}\right) \frac{-\pi}{D^R(\epsilon + \omega/2) + D^R(\epsilon - \omega/2) + 1/\tau} \left[\frac{\epsilon^2 - \omega^2/4 + \Delta^2}{D^R(\epsilon + \omega/2)D^R(\epsilon - \omega/2)} + 1 \right] \right. \\ & - \tanh\left(\frac{\epsilon + \omega/2}{2T}\right) \frac{-\pi}{D^A(\epsilon + \omega/2) + D^A(\epsilon - \omega/2) + 1/\tau} \left[\frac{\epsilon^2 - \omega^2/4 + \Delta^2}{D^A(\epsilon + \omega/2)D^A(\epsilon - \omega/2)} + 1 \right] \\ & \left. + \left[\tanh\left(\frac{\epsilon + \omega/2}{2T}\right) - \tanh\left(\frac{\epsilon - \omega/2}{2T}\right) \right] \times \frac{-\pi}{D^R(\epsilon + \omega/2) + D^A(\epsilon - \omega/2) + 1/\tau} \left[\frac{\epsilon^2 - \omega^2/4 + \Delta^2}{D^R(\epsilon + \omega/2)D^A(\epsilon - \omega/2)} + 1 \right] \right\}, \end{aligned} \quad (3)$$

where $\sigma_D \equiv (2/3)N_f e^2 v_f^2 \tau$ is the Drude result for the d.c. conductivity of the normal metallic state, and $D^{R,A}(\epsilon)$ are the retarded (R) and advanced (A) functions defined by $D^{R,A}(\epsilon) \equiv \sqrt{\Delta^2 - (\epsilon \pm i\eta)^2}$, where $\eta \rightarrow 0^+$ and the upper

and lower signs correspond to the retarded (R) and advanced (A) functions, respectively, that determine the corresponding non-equilibrium propagators. Note that there is no “Dynes parameter” introduced into the theoretical formalism, and

the impurity scattering rate drops out of the equilibrium propagators, and thus $D^{\text{R.A.}}(\omega)$, for isotropic superconductors with non-magnetic impurities (Anderson's theorem). As a result the impurity scattering rate $1/\tau$ appears only explicitly as shown in the kernel of the conductivity in Eq. (3) [14]. The three lines of this equation correspond, respectively, to the retarded, advanced and anomalous contributions to the nonequilibrium Keldysh kernel for the conductivity. It is straight-forward to show that the normal-state limit ($\Delta \rightarrow 0$) of Eq. (3) reduces to the frequency-dependent Drude conductivity,

$$\sigma_n = \sigma_{\text{D}} \frac{1 + i\omega\tau}{1 + (\omega\tau)^2}. \quad (4)$$

The imaginary part of the a.c. conductivity determines the normal metal skin depth. For $\omega\tau \ll 1$, $\delta(\omega) = c/\sqrt{2\pi\omega\sigma_{\text{D}}}$. The penetration of the EM field in the normal state, and thus the frequency shift of the cavity *relative* to the geometric resonant frequency for a perfect conducting cavity, is independent of temperature in the vicinity near T_c . This shift determines the reference frequency for changes in the resonant frequency below T_c . The penetration depth changes rapidly as a function of temperature at the onset of superconductivity, leading to rapid changes in the resonant frequency, including anomalies very close to T_c . The full analysis of both field penetration and the change in the resonant frequency of the cavity is presented in the following sections.

III. SURFACE IMPEDANCE OF SRF CAVITIES

To compare with experimental reports it is convenient to introduce the complex surface impedance of the vacuum-superconducting interface,

$$Z_s \equiv Z_0 \frac{E_{\parallel}(z=0)}{H_{\parallel}(z=0)}, \quad (5)$$

where $E_{\parallel}(z=0)$ and $H_{\parallel}(z=0)$ are the electric and magnetic field components in the plane of the interface and evaluated just below the metal surface. The prefactor, $Z_0 \equiv 4\pi/c = 376.7 \Omega$, is the so-called impedance of the vacuum. Maxwell's equations, combined with Eq. (1), yield the surface impedance in terms of the complex a.c. conductivity [18],

$$Z_s = Z_0 \sqrt{\frac{\omega}{4\pi i\sigma(\omega)}}. \quad (6)$$

Equation (6) is valid for the surface response of superconductors in the local limit $\ell \ll \xi \ll \lambda$, where ℓ , ξ , and λ are the mean free path, coherence length, and the London penetration depth, respectively. The same relationship holds for the surface impedance of the normal metal and the Drude conductivity, $Z_n = Z_0 \sqrt{\frac{\omega}{4\pi i\sigma_n(\omega)}}$. The conductivity and surface impedance are complex functions of frequency, temperature and scattering rate. Expressing $Z_s = R_s - iX_s$ in terms of the surface resistance, R_s and surface reactance, X_s , we can relate these quantities to the real and imaginary components of the conductivity, $\sigma = \sigma_1 + i\sigma_2$.

The relations connecting R_s and X_s to $\sigma_{1,2}$ simplify in the low-frequency limit, $\omega\tau \ll 1$, which is applicable to the analysis presented below for Nb SRF cavities with intermediate

to strong disorder. In this limit $X_n \simeq R_n = Z_0 \sqrt{f/4\sigma_{\text{D}}}$, and

$$\frac{R_s}{R_n} = \frac{\sigma_{n1}^{1/2}}{(\sigma_1^2 + \sigma_2^2)^{1/4}} \times \left[\cos\left(\frac{1}{2} \arctan \frac{\sigma_2}{\sigma_1}\right) - \sin\left(\frac{1}{2} \arctan \frac{\sigma_2}{\sigma_1}\right) \right], \quad (7)$$

$$\frac{X_s}{R_n} = \frac{\sigma_{n1}^{1/2}}{(\sigma_1^2 + \sigma_2^2)^{1/4}} \times \left[\cos\left(\frac{1}{2} \arctan \frac{\sigma_2}{\sigma_1}\right) + \sin\left(\frac{1}{2} \arctan \frac{\sigma_2}{\sigma_1}\right) \right]. \quad (8)$$

A. δf and Q of SRF cavities

Slater solved Maxwell's equations in a hollow cavity with small damping and derived the expression for the quality factor and the frequency shift from an ideal cavity as [15]

$$\frac{1}{Q} + 2i \frac{\Delta\omega_a}{\omega_a} = i \frac{c}{\omega_a} \frac{\int_S (\mathbf{n} \times \mathbf{E}) \cdot \mathbf{H}_a da}{\int \mathbf{E} \cdot \mathbf{E}_a dv} - \frac{c}{\omega_a} \frac{\int_{S'} (\mathbf{n} \times \mathbf{H}) \cdot \mathbf{E}_a da}{\int \mathbf{E} \cdot \mathbf{E}_a dv} + \frac{4\pi}{\omega_a} \frac{\int \mathbf{j} \cdot \mathbf{E}_a dv}{\int \mathbf{E} \cdot \mathbf{E}_a dv}, \quad (9)$$

where ω_a is the angular frequency of the a th mode in an ideal resonant cavity, \mathbf{E}_a and \mathbf{H}_a are the a th mode of the electric and magnetic fields, respectively, S and S' denote conductive and insulating surfaces, respectively, and \mathbf{n} is the outer normal to the surface. See App. A for details. Here we consider only damping from metallic walls of an SRF cavity, and thus we neglect the second term on the right-hand side of Eq. (9). We also can neglect the third term since the source current vanishes in the vacuum region. We substitute $\mathbf{n} \times \mathbf{E} = (Z_s/Z_0)\mathbf{H}$ into Eq. (9), and assume that \mathbf{H} is given by the magnetic field of the a th mode [15]. Finally, we use $\int \mathbf{E} \cdot \mathbf{E}_a dv = i \int \mathbf{H} \cdot \mathbf{H}_a dv$ from App. A.

$$\mathbf{H} = \mathbf{H}_a \int \mathbf{H} \cdot \mathbf{H}_a dv = -i \mathbf{H}_a \int \mathbf{E} \cdot \mathbf{E}_a dv. \quad (10)$$

As a result we obtain the quality factor and frequency shift in terms of the surface impedance

$$\frac{1}{Q} + 2i \frac{\Delta\omega_a}{\omega_a} = \frac{Z_s}{G}, \quad (11)$$

where G is the geometric factor of the cavity defined by $G \equiv Z_0 \omega_a / c \int_S \mathbf{H}_a^2 da$. Using the Eq. (11) Slater calculated the frequency shift and quality factor for a normal-metal-vacuum interface [15]. Furthermore, using $\omega_a = 2\pi f_a$ and subtracting the normal frequency shift from the superconducting frequency shift, we obtain relation between the frequency shift of the superconducting cavity measured relative to the normal-state resonance frequency and the corresponding surface reactances,

$$\delta f = \frac{f}{2G} (X_n - X_s), \quad G = Z_0 \frac{2\pi f}{c} \frac{\int \mathbf{H}^2 dv}{\int_S \mathbf{H}^2 da}. \quad (12)$$

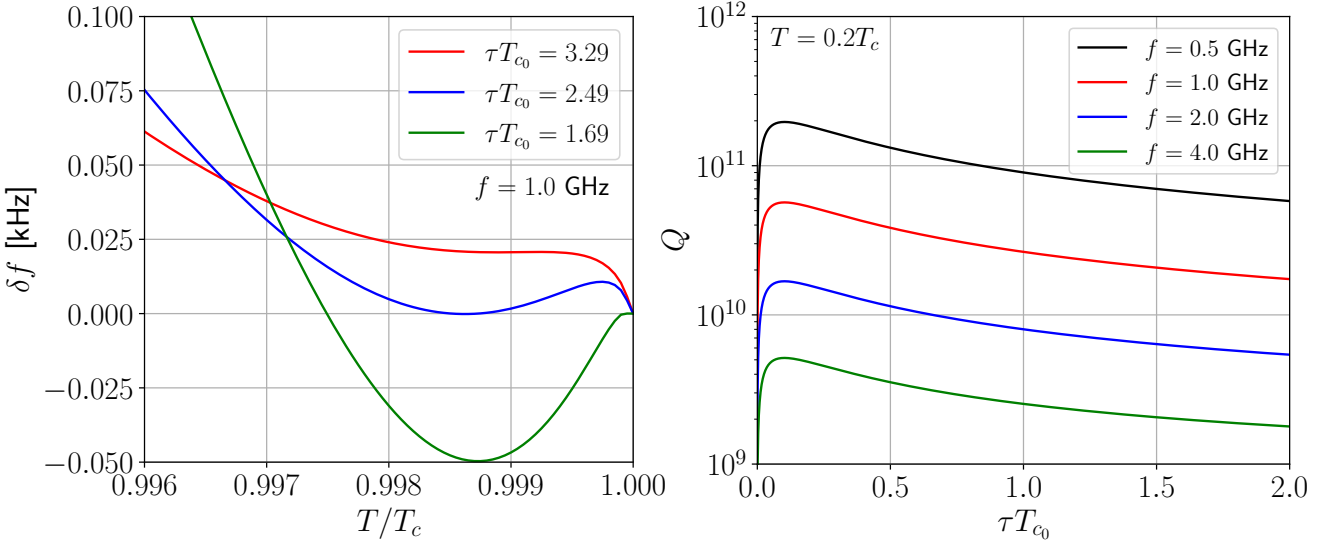


FIG. 2. Left panel: Temperature dependence of the frequency shift δf for relatively clean cavities with $f = 1.0\text{GHz}$ near T_c . Right panel: The effect of disorder on Q at $T = 0.2T_c$. Note the maximum Q is near $\tau T_{c_0} \approx 0.1$, i.e. intermediate disorder.

The subscript a for the relevant mode is omitted hereafter. This formula is used to calculate the frequency shift of a superconducting sample in a cavity. We also obtain the quality factor from the surface resistance,

$$Q = \frac{G}{R_s}. \quad (13)$$

B. Material parameters for Nb

From the Drude conductivity the normal-state surface resistance can be related to the scattering rate, $1/\tau$, and the plasma frequency, ω_p , by $\sigma_d = \frac{\omega_p^2 \tau}{4\pi}$. Thus we have,

$$R_n = \frac{Z_0}{\omega_p} \sqrt{\frac{\pi f}{\tau}}. \quad (14)$$

The plasma frequency, $\omega_p = \sqrt{(8\pi/3)N_f e^2 v_f^2}$, is also simply related to the zero-temperature limit of the London penetration depth for pure Nb, $\lambda_L = c/\omega_p$, both expressed in terms of the electron charge, e , density of states N_f , Fermi velocity, v_f . We adopt the Fermi velocity reported in Ref. 20, $v_f = 0.26 \times 10^8 \text{ cm/s}$, and the London penetration depth from Ref. 10. With these parameters we calculate the density of states, $N_f = 0.101 \text{ eV}^{-1} \text{ \AA}^{-3}$, and the plasma frequency, $\omega_p = c/\lambda_L = 9.08 \times 10^6 \text{ GHz}$. We use these results and the normal-state surface resistance as input to calculations of the frequency shift and quality factor of SRF cavities.

IV. ANOMALIES IN δf AND MAXIMUM Q

We highlight the two key features of the cavity response for relatively clean SRF cavities with $f = 1.0\text{GHz}$ and $G = 250\Omega$: (i) the non-monotonic behavior of the frequency shift and its sensitivity to the level of disorder, and (ii) the maximum in the quality factor at finite levels of disorder. Both features are shown in Fig. 2. The left panel shows three general features in δf for temperatures very near T_c : (a) a negative shift, then a recovery (dip feature) for $\tau T_{c_0} = 1.69$, (b) a

positive shift, then a decline and recovery (bump feature) for $\tau T_{c_0} = 2.49$, and finally (c) a rapid increase followed by a slow recovery (plateau feature) for $\tau T_{c_0} = 3.29$, where $T_{c_0} = 9.33\text{K}$ is the transition temperature of pure Nb [17].

All three types of frequency shift anomalies are observed in Nb SRF cavities depending on the levels of disorder [7]. We also find that the quality factor Q has a peak of upper convexity as a function of the mean scattering time, confirming results by other authors [21]. Thus, the maximum Q in SRF cavities occurs for intermediate levels of disorder, and is suppressed in dirty cavities due to the pair breaking.

A. Analysis of Nb in a Cooper Cavity at $f = 60\text{GHz}$

Figure 3 shows the temperature dependence of the frequency shift and quality factor for a Nb sample embedded in a copper cavity. The points are experimental data calculated from the surface resistance and reactance reported by Klein et al. [10]. We have calculated the a.c. conductivity based on the weak coupling limit for the conductivity given by Eq. (3). We then calculate quality factor and frequency shift obtained from the conductivity and compare with the experimental results for a Niobium sample in a copper cavity as reported and measured by Klein et al. [10]. The resonance frequency and the resonator constant of the copper cavity used here were $f = 60\text{GHz}$ and $v = Z_0/2G = 0.0458$, respectively. The solid lines are the theoretical results. The monotonic increase in Q is expected, although the comparison between theory and experiment is not perfect, but the experimental data does have significant scatter [10]. For the frequency shift the comparison is much better. In addition we obtain theoretically the negative frequency shift anomaly that is implicit in the experimental data for the reactance in the close vicinity of T_c . The inset shown in the left panel of Fig. 3 shows a zoom-in of the region very near T_c , with the exact result for the shift shown as the solid line, which is in agreement with the data from Klein et al. [10]. The dashed line is the result obtained by perturbation theory in $\Delta^2 \propto (T_c - T)$, which is valid only for $\omega > 2\Delta(T)$. In this region $\sigma_1^{(2)}$ defined by Eq. (B2) is negative since pair breaking results from absorption in this window near T_c .

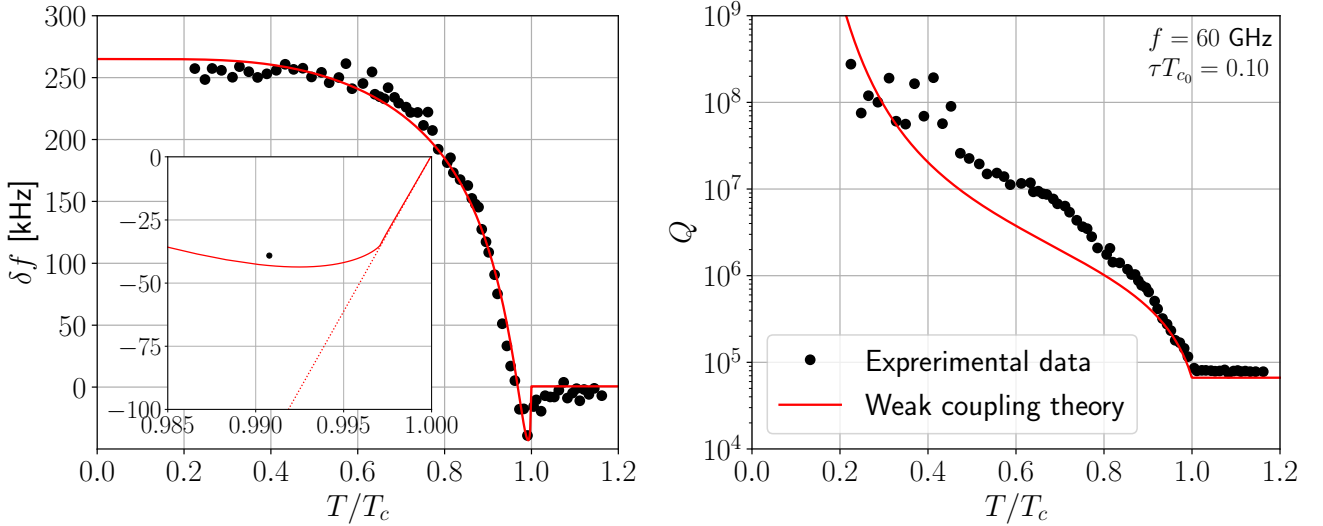


FIG. 3. Frequency shift δf (left) and quality factor Q (right) of a Nb sample embedded in a copper cavity as a function of temperature for a cavity with resonant frequency $f = 60$ GHz. The points are experimental data calculated from the surface impedance reported by Klein et al. [10]. The solid lines are calculated based on Eqs. (3), (6) and (11) with the scattering rate $1/\tau T_{c_0} = 10.0$. Inset: zoomed-in plot of δf very near T_c . The dashed line is based on the perturbative expansion of the conductivity in $\Delta^2 \propto (T_c - T)$ given by Eq. (B5a).

In addition, $\sigma_2^{(2)} - \sigma_1^{(2)} > 0$ implying that the frequency shift is negative just below T_c . The authors of Ref. 10 compared their results with calculations of the conductivity based on Mattis-Bardeen theory in the dirty limit [22]. They adjusted T_c and the gap to fit the experimental data. Our analysis incorporates the roles of gap anisotropy and disorder to account for both the suppression of T_c and the gap amplitude in order to obtain a consistent theory for the effects of disorder on T_c , Δ and the conductivity as a function of the quasiparticle scattering rate $1/\tau$. Our analysis yields $1/\tau T_{c_0} \simeq 10$, implying that the samples studied were in the cross-over region between weak and strong disorder [23].

B. Effects of anisotropy and disorder on T_c , Δ and $\sigma(\omega, T)$

Niobium is an anisotropic superconductor belonging to the identity representation of the cubic point group. Thus, the gap amplitude varies with position (Fermi momentum) on the Fermi surface, but is otherwise invariant under the point group symmetry. The combination of anisotropy of the Cooper pair amplitude defined on the Fermi surface in momentum space and elastic scattering by non-magnetic disorder, from either impurities or structural defects, leads to the violation of Anderson's theorem, i.e. the suppression of pair formation and reduction of T_c , as well as the maximum excitation gap. The suppression of T_c has been calculated and is given by [17]

$$\ln \frac{T_{c_0}}{T_c} = \mathcal{A} \times 2\pi T_c \sum_{\varepsilon_n > 0}^{\infty} \left(\frac{\hbar/\tau}{\varepsilon_n(\varepsilon_n + \frac{1}{2}\hbar/\tau)} \right), \quad (15)$$

where $\varepsilon_n = (2n + 1)\pi T_c$ are the Matsubara energies evaluated at the transition temperature for disordered Nb. The gap amplitude has the general form, $\Delta(\mathbf{p}) = \Delta(T)\mathcal{Y}(\mathbf{p})$, where $\mathcal{Y}(\mathbf{p})$ is Cooper pair amplitude as a function of position \mathbf{p} on the Fermi surface, normalized to $\int d\mathbf{p} |\mathcal{Y}(\mathbf{p})|^2 = 1$. The integration is an average over the Fermi surface. In the limit $T \rightarrow T_c$ the Cooper pair amplitude, $\mathcal{Y}(\mathbf{p})$, is the eigenfunction of the linearized gap equation that determines the T_{c_0} in the clean limit. The anisotropy parameter in Eq. (15) is

defined by the limit

$$\mathcal{A} = \lim_{T \rightarrow T_{c_0}} \frac{\langle |\Delta(\mathbf{p})|^2 \rangle - \langle |\Delta(\mathbf{p})| \rangle^2}{\langle |\Delta(\mathbf{p})|^2 \rangle} = 1 - \langle |\mathcal{Y}(\mathbf{p})|^2 \rangle, \quad (16)$$

where $\langle \dots \rangle = \int d\mathbf{p} \dots$ is the the Fermi surface average with $\langle 1 \rangle = 1$ and $\mathcal{Y}(\mathbf{p})$ is normalized as $\langle |\mathcal{Y}(\mathbf{p})|^2 \rangle = 1$. In general the anisotropy factor \mathcal{A} can range from $\mathcal{A} = 0$ for an isotropic s -wave superconductor, to the other extreme of $\mathcal{A} = 1$, i.e. $\langle |\Delta(\mathbf{p})| \rangle \equiv 0$, characteristic of unconventional superconductors that break the point group symmetry. For conventional, anisotropic superconductors $0 < \mathcal{A} < 1$, and for Niobium we use the results of a recent first-principles calculation of the gap anisotropy parameter for pure single crystalline Niobium of $\mathcal{A} = 0.037$ and $T_{c_0} = 9.33$ K [17]. Figure 11 in Ref. [17] shows the suppression of T_c for Nb as a function of the dimensionless scattering rate $1/2\pi\tau T_{c_0}$.

While the role of anisotropy is essential in accounting for the variations of T_c and the excitation gap with disorder, the a.c. conductivity, at least for fully gapped conventional superconductors, is otherwise insensitive to the gap anisotropy for frequencies, $\hbar\omega \ll 2\Delta(\mathbf{p})$. Thus, we neglected the explicit dependence on gap anisotropy in Eq. (3) for the conductivity, but we include the implicit dependence on anisotropy in the suppression of T_c and $\Delta(T) \equiv \sqrt{\langle |\Delta(\mathbf{p})|^2 \rangle}$. We can calculate $\Delta(T)$ from the BCS gap equation, expressed below in terms of the zero temperature gap, $\Delta_0 = \pi e^{-\gamma} T_c$ where $\gamma = 0.57721 \dots$ is the Euler-Mascheroni constant,

$$\ln \frac{\Delta}{\Delta_0} = 2 \int_0^{\infty} d\xi \frac{1}{\sqrt{\xi^2 + \Delta^2}} \frac{1}{e^{\sqrt{\xi^2 + \Delta^2}/2T} + 1}. \quad (17)$$

The solution for the BCS gap function is well described by the interpolation formula

$$\Delta(T, T_c) = \Delta_0 \tanh \left(\frac{\pi T_c}{\Delta_0} \sqrt{\frac{2}{3} \frac{\Delta C}{C_n(T_c)} \frac{T_c - T}{T}} \right) \Theta(T_c - T), \quad (18)$$

where $\Delta C \equiv C(T_c) - C_n(T_c) = 12C_n(T_c)/7\zeta(3)$ is the jump in the heat capacity at T_c , with $C(T_c)$ and $C_n(T_c)$ denoting the

superconducting and normal-state heat capacities, respectively, and $\zeta(3) = 1.20205\cdots$ is the Riemann zeta function. We use Eq. (18) in the analysis to follow to incorporate the effects of inhomogeneous disorder on T_c and $\Delta(T)$.

C. Analysis of N-doped Nb SRF Cavities

Detailed measurements of the temperature dependence of the frequency shift δf are reported for four Nitrogen-doped Nb SRF cavities with characteristic frequencies of $f_0 = \{0.65, 1.3, 2.6, 3.9\}$ GHz, including the the region of temperature very near T_c [7]. The experimental data, taken from Ref. 7 and reproduced in Fig. 4, shows a negative frequency shift anomaly in a narrow region of temperature that depends of f_0 , T_c and $1/\tau$, as well as inhomogeneity of the disorder and its effect on T_c and $\Delta(T, T_c)$ [24] Table I summarizes the key parameters of the four N-doped Nb cavities, including the spread in T_c measured locally for each cavity [25].

We calculated the conductivity from Eq. (3), adjusting the scattering rate $1/\tau$ to obtain an optimal fit for $\delta f(T)$ for each cavity. The geometric factors for each of the Tesla cavities were provided by the Fermilab team: $G = 255 \Omega$ for $f = 0.65$ GHz, $G = 270 \Omega$ for $f = 1.3$ GHz, $G = 270 \Omega$ for $f = 2.6$ GHz, and $G = 293 \Omega$ for $f = 3.9$ GHz [25]. From this input and our theoretical formulation we calculate the a.c. conductivity and obtain the negative frequency shift anomaly of the right magnitude. However, a single parameter description of the disorder, i.e. *homogeneous disorder*, does not accurately predict the temperature at the minimum of δf . From the spread in T_c for each cavity we construct a distribution profile, $\rho(T_c)$ representing the inhomogeneity of the disorder for each cavity. Introducing T_c^{\max} and T_c^{\min} , we express the average and variance in the Gaussian distribution of T_c as $\mu = T_c^{\text{av}} \equiv (T_c^{\max} + T_c^{\min})/2$ and $\mu_2 = [(T_c^{\text{av}} - T_c^{\min})/3]^2$, respectively. We determine T_c^{\max} and T_c^{\min} as the two key fitting parameters so that the calculation of the frequency shift best fits the experimental data. The corresponding distribution for the scattering rate can be obtained using Eq. (15). The details of this analysis for each cavity is described in App. C with the corresponding plots of the distributions of T_c , $1/\tau$ as well as the inhomogeneously broadened gap function defined by

$$\Delta(T) = \Delta_0 \sqrt{\int_{-\infty}^{+\infty} dT_c \rho(T_c) \Delta^2(T, T_c)}. \quad (19)$$

Note that overall magnitude of the disorder as well as the spread varies among the cavities, although all exhibit a similar level of disorder with typical scattering rates ranging between $\sim 4 - 6 \text{ ps}^{-1}$. Note also that the inhomogeneously broadened gap function rises more slowly in temperature due to the spread in T_c , leading to a change in the position of the minimum in the frequency shift anomaly. We use the average value of $1/\tau$ obtained from $\tilde{\rho}(1/\tau)$ shown in Fig. 6 in Eqs.(3) and (14) in order to calculate the conductivity and normal-state surface resistance. In particular, $\bar{\tau}T_{c0} = 0.214, 0.273, 0.300$, and 0.299 for $f = 0.65$ GHz, 1.3 GHz, 2.6 GHz, and 3.9 GHz, respectively, where $1/\bar{\tau}$ is the average of $1/\tau$. Note that we can also obtain the average of $1/\tau$ by solving Eq. (15) at the average value of T_c . Table I shows T_c^{\max} , T_c^{\min} , and R_n , used for the calculation based on the weak coupling theory with the spread in T_c , as well as the measured values from Ref.25, for the four N-doped Nb SRF

TABLE I. T_c^{\max} , T_c^{\min} , and R_n used for the calculation based on the weak coupling theory with the spread in T_c (second row), and measured by Bafia et al. (third row), for the Nb SRF cavities with each different resonance frequency.

f [GHz]	Theory				Experiment			
	0.65	1.3	2.6	3.9	0.65	1.3	2.6	3.9
T_c^{\max} [K]	8.965	9.004	9.044	9.032	9.005	8.907	9.081	9.165
T_c^{\min} [K]	8.895	8.976	8.980	8.990	8.975	8.87	9.041	9.15
R_n [mΩ]	4.471	5.601	7.554	9.272	4.364	5.425	6.95	8.93

cavities.[26] As shown in Table I, the experimental and theoretical values for T_c^{\max} , T_c^{\min} , and R_n are in good agreement with each other.

Figure 4 shows the temperature dependence of the frequency shift of the four N-doped Nb SRF cavities measured by Bafia et al. [7], and the comparison with our calculated result based on Eq. (12) and weak-coupling theory for the conductivity, including inhomogeneous disorder with the spread in T_c for the N-doped Nb SRF cavities. The origin of the negative frequency shift anomaly onsetting at T_c is the same as described earlier in the context of the analysis of the results of Klein et al. [10]. The negative shift and ‘dip feature’ in the frequency shift follows from the change in the surface reactance defined in Eq.(8); X_s/R_n , which is proportional to the frequency shift with the negative proportionality coefficient, is the product of $[(\sigma_1/\sigma_{1n})^2 + (\sigma_2/\sigma_{1n})^2]^{-1/4}$ and $\cos[\frac{1}{2} \arctan(\sigma_2/\sigma_1)] + \sin[\frac{1}{2} \arctan(\sigma_2/\sigma_1)]$ as seen in Eq. (8), and the former decreases and the latter increases as temperature is lowered below T_c . Therefore, X_s/R_n and the frequency shift have a peak near T_c when σ_2/σ_1 in the latter increases sharply below T_c .

We also see from Eq. (7) that the ratio σ_2/σ_1 is important in determining the temperature and disorder dependence of the quality factor. In particular, R_s/R_n , which is inversely proportional to the quality factor, is the product of $[(\sigma_1/\sigma_{1n})^2 + (\sigma_2/\sigma_{1n})^2]^{-1/4}$ and $\cos[\frac{1}{2} \arctan(\sigma_2/\sigma_1)] - \sin[\frac{1}{2} \arctan(\sigma_2/\sigma_1)]$, both the former and latter decrease as the temperature drops below T_c , and the latter is the dominant contribution to R_s/R_n . Thus, since R_s/R_n decreases more drastically when σ_2/σ_1 increases more sharply below T_c , the quality factor increases.

In summary, both the quality factor and the negative frequency shift near T_c are enhanced by the large value of σ_2 for intermediate levels of disorder. To check if our theory also predicts the experimentally reported quality factor $Q(T)$, we compare our theory with the data reported in Fig. 2 of the Supplemental Material of Ref. 7. Figure 5 shows the comparison for the temperature dependence of the frequency shift and quality factor of a different N-doped Nb SRF cavity with $f = 1.3$ GHz. The data points were obtained from the surface impedance reported in the Supplemental Material for Ref. 7, and the solid lines are the calculated results with $\tau T_{c0} = 0.17$ based on weak coupling theory and homogeneous disorder, i.e. neglecting the spread in $1/\tau$ and T_c . The frequency shift is in close agreement, while the quality factor obtained by our theory is not perfect, but in reasonable agreement with that of Ref. 7. If the low-temperature behavior shown in the experimental result for $Q(T)$ is reproducible then there is likely low-energy sub-gap states present in this cavity that are not present in the theory we present.

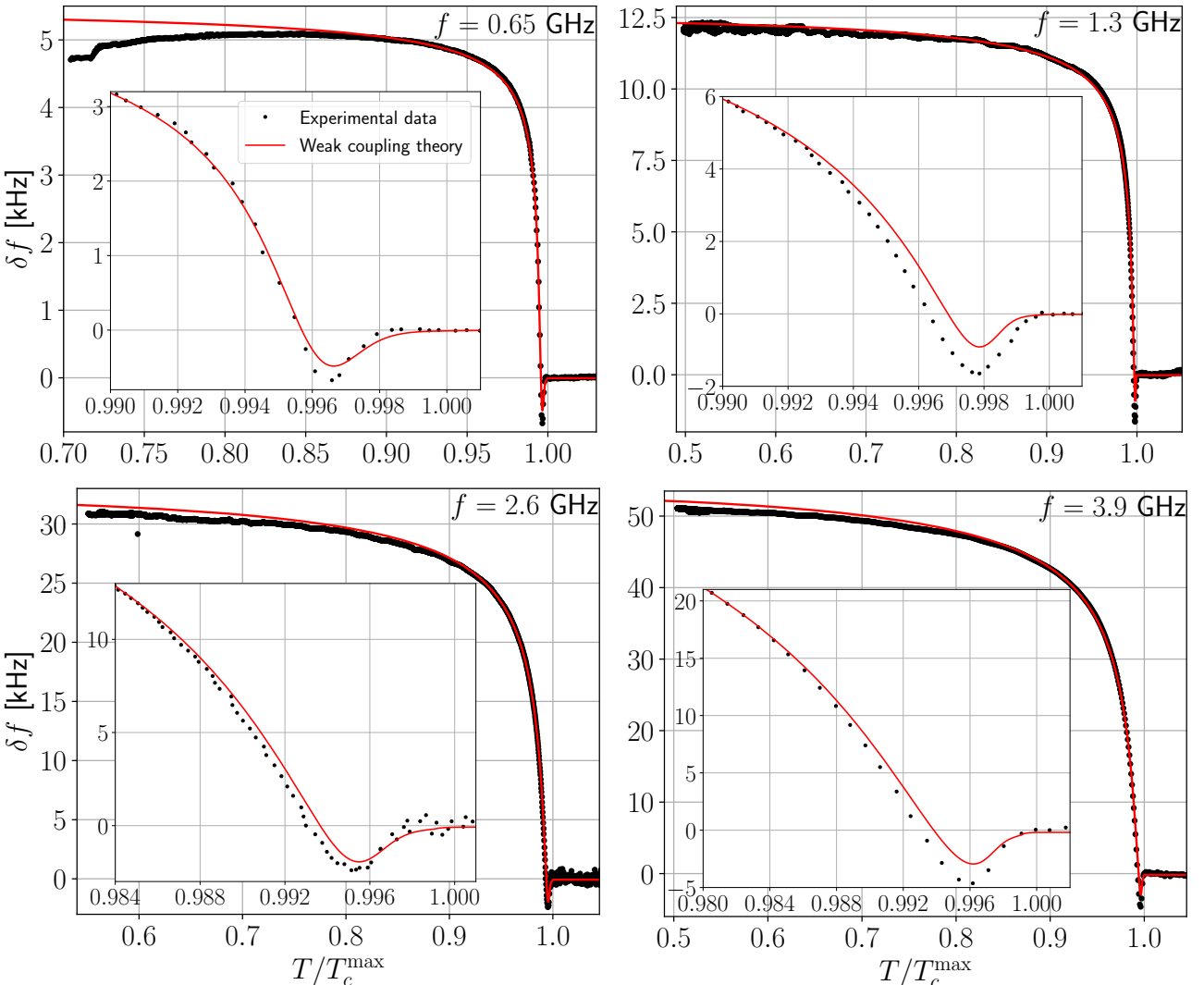


FIG. 4. Temperature dependence of the frequency shift δf of the Nb SRF cavities with each different resonance frequency, $f = 0.65$ GHz (upper left), 1.3 GHz (upper right), 2.6 GHz (lower left), and 3.9 GHz (lower right), near T_c . The black points are the measured values extracted from and reported by Bafia et al. [7], and the red lines are our calculations based on weak coupling theory with inhomogeneous disorder. Each inset is the zoomed-in region near T_c .

V. CONCLUSIONS

We developed a theory and computational method to calculate the frequency shift δf , quality factor Q , and surface impedance Z_s , from the a.c. conductivity σ of disordered superconducting RF cavities based on the quasiclassical theory of superconductivity in the weak coupling limit, combined with Maxwell's equations. We showed that the observable properties of these cavities are well described by the weak coupling theory with an anisotropic gap function and scattering by a non-magnetic distribution of disorder. We show that δf vs $T \lesssim T_c$ and T_c vs $1/\tau$ provide sensitive measures of the quality of disordered Nb cavities. Our analysis also indicates that even "state of the art" N-doped Nb SRF cavities can be further improved in terms of Q by reducing the overall level of disorder. However, there is a level of disorder that is desirable because the quality factor has a maximum as a function of the quasiparticle-impurity scattering rate, with the largest Q corresponding to intermediate disorder. For strong disorder, i.e. the dirty limit, pair breaking limits the Q .

VI. ACKNOWLEDGEMENTS

We thank Daniel Bafia, Anna Grassellino, Alex Romanenko and John Zasadzinski for many discussions on their experimental work on SRF cavities, and for motivating this study. The research of HU and MZ was supported by National Science Foundation Grant PHY-1734332 and the Northwestern-Fermilab Center for Applied Physics & Superconducting Technologies. The work of JAS is supported by the U.S. Department of Energy, Office of Science, National Quantum Information Science Research Centers, Superconducting Quantum Materials and Systems Center (SQMS) under contract number DE-AC02-07CH11359.

Appendix A: Slater's Method

We consider the electromagnetic field in a hollow cavity to derive Eq. (9) obtained by Slater [15]. We first expand the

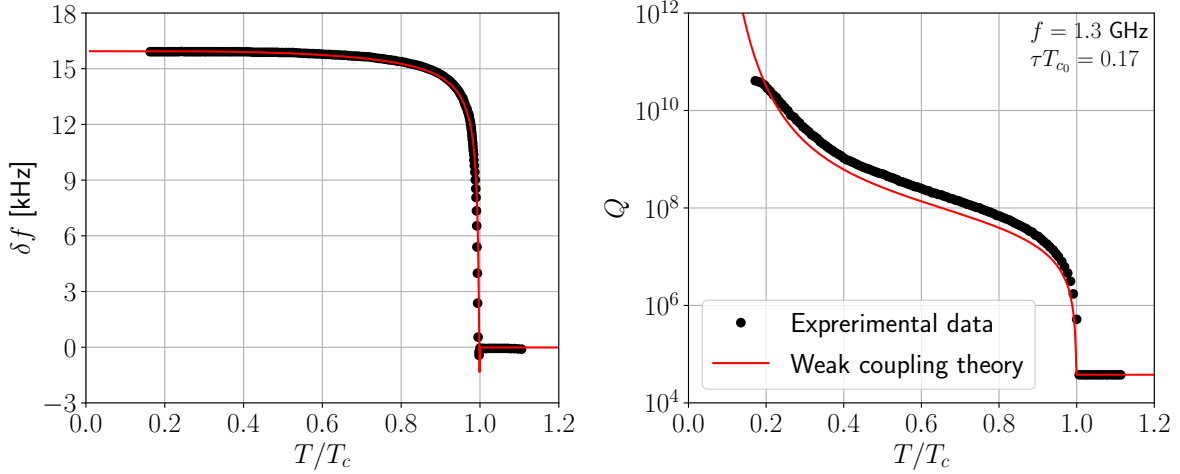


FIG. 5. Frequency shift δf (left) and quality factor Q (right) of an SRF cavity with nominal resonant frequency $f_0 = 1.3$ GHz as a function of temperature. The points are experimental data calculated from the surface impedance reported by Bafia et al. [7], and the lines are theoretical results calculated with mean scattering time $\tau T_{c0} = 0.17$ based on weak coupling theory.

EM fields as

$$\mathbf{E} = \sum_a \left(\mathbf{E}_a \int \mathbf{E} \cdot \mathbf{E}_a dv + \mathbf{F}_a \int \mathbf{E} \cdot \mathbf{F}_a dv \right), \quad (\text{A1a})$$

$$\mathbf{H} = \sum_a \mathbf{H}_a \int \mathbf{H} \cdot \mathbf{H}_a dv, \quad (\text{A1b})$$

$$\mathbf{j} = \sum_a \left(\mathbf{E}_a \int \mathbf{j} \cdot \mathbf{E}_a dv + \mathbf{F}_a \int \mathbf{j} \cdot \mathbf{F}_a dv \right), \quad (\text{A1c})$$

$$\rho = \sum_a \psi_a \int \rho \psi_a dv, \quad (\text{A1d})$$

using the solenoidal vector functions \mathbf{E}_a and \mathbf{H}_a , which satisfy the following equations: $k_a \mathbf{E}_a = \nabla \times \mathbf{H}_a$ and $k_a \mathbf{H}_a = \nabla \times \mathbf{E}_a$, and the irrotational vector function \mathbf{F}_a , which is the gradient of a scalar function ψ_a , $k_a \mathbf{F}_a = \nabla \psi_a$, where k_a is the propagation constant associated with the a th mode as discussed below. These functions satisfy the normalization and orthogonality conditions as

$$\int \mathbf{E}_a \cdot \mathbf{E}_b dv = \delta_{ab}, \quad \int \mathbf{H}_a \cdot \mathbf{H}_b dv = \delta_{ab}, \quad (\text{A2a})$$

$$\int \mathbf{F}_a \cdot \mathbf{F}_b dv = \delta_{ab}, \quad \int \psi_a \psi_b dv = \delta_{ab}, \quad (\text{A2b})$$

$$\int \mathbf{E}_a \cdot \mathbf{F}_b dv = 0, \quad (\text{A2c})$$

wave equations,

$$\nabla^2 \mathbf{E}_a + k_a^2 \mathbf{E}_a = \mathbf{0}, \quad \nabla^2 \mathbf{H}_a + k_a^2 \mathbf{H}_a = \mathbf{0}, \quad (\text{A3a})$$

$$\nabla^2 \psi_a + k_a^2 \psi_a = 0, \quad (\text{A3b})$$

and boundary conditions,

$$\mathbf{n} \times \mathbf{E}_a = \mathbf{0}, \quad \mathbf{n} \cdot \mathbf{H}_a = 0, \quad \mathbf{n} \times \mathbf{F}_a = \mathbf{0}, \quad \psi_a = 0 \quad \text{on } S, \quad (\text{A4a})$$

$$\mathbf{n} \times \mathbf{H}_a = \mathbf{0}, \quad \mathbf{n} \cdot \mathbf{E}_a = 0, \quad \mathbf{n} \times \mathbf{F}_a = \mathbf{0}, \quad \psi_a = 0 \quad \text{on } S', \quad (\text{A4b})$$

where \mathbf{n} is the outer normal to the surface, and S and S' are the conductive and insulating surfaces, respectively. We can also expand $\nabla \times \mathbf{E}$, $\nabla \times \mathbf{H}$, and $\nabla \cdot \mathbf{E}$ in terms of the functions

\mathbf{E}_a , \mathbf{H}_a , \mathbf{F}_a , and ψ_a as [15],

$$\begin{aligned} \nabla \times \mathbf{E} &= \sum_a \mathbf{H}_a \int (\nabla \times \mathbf{E}) \cdot \mathbf{H}_a dv \\ &= \sum_a \mathbf{H}_a \left[k_a \int \mathbf{E} \cdot \mathbf{E}_a dv + \int_S (\mathbf{n} \times \mathbf{E}) \cdot \mathbf{H}_a da \right], \end{aligned} \quad (\text{A5a})$$

$$\begin{aligned} \nabla \times \mathbf{H} &= \sum_a \mathbf{E}_a \int (\nabla \times \mathbf{H}) \cdot \mathbf{E}_a dv \\ &= \sum_a \mathbf{E}_a \left[k_a \int \mathbf{H} \cdot \mathbf{H}_a dv + \int_{S'} (\mathbf{n} \times \mathbf{H}) \cdot \mathbf{E}_a da \right], \end{aligned} \quad (\text{A5b})$$

$$\nabla \cdot \mathbf{E} = \sum_a \psi_a \int (\nabla \cdot \mathbf{E}) \psi_a dv = - \sum_a \psi_a k_a \int \mathbf{E} \cdot \mathbf{F}_a dv. \quad (\text{A5c})$$

Substituting Eqs. (A1) and (A5) into Maxwell's equations, we obtain

$$\begin{aligned} k_a \int \mathbf{E} \cdot \mathbf{E}_a dv + \frac{1}{c} \frac{d}{dt} \int \mathbf{H} \cdot \mathbf{H}_a dv \\ = - \int_S (\mathbf{n} \times \mathbf{E}) \cdot \mathbf{H}_a da, \end{aligned} \quad (\text{A6a})$$

$$\begin{aligned} k_a \int \mathbf{H} \cdot \mathbf{H}_a dv - \frac{1}{c} \frac{d}{dt} \int \mathbf{E} \cdot \mathbf{E}_a dv \\ = \frac{4\pi}{c} \int \mathbf{j} \cdot \mathbf{E}_a dv - \int_{S'} (\mathbf{n} \times \mathbf{H}) \cdot \mathbf{E}_a da, \end{aligned} \quad (\text{A6b})$$

$$- \frac{1}{c} \frac{d}{dt} \int \mathbf{E} \cdot \mathbf{F}_a dv = \frac{4\pi}{c} \int \mathbf{j} \cdot \mathbf{F}_a dv, \quad (\text{A6c})$$

$$- k_a \int \mathbf{E} \cdot \mathbf{F}_a dv = 4\pi \int \rho \psi_a dv. \quad (\text{A6d})$$

We also obtain separate equations for $\int \mathbf{E} \cdot \mathbf{E}_a dv$ and $\int \mathbf{H} \cdot \mathbf{H}_a dv$ from Eqs. (A6a) and (A6b) as

$$\begin{aligned} & \frac{1}{c^2} \frac{d^2}{dt^2} \int \mathbf{E} \cdot \mathbf{E}_a dv + k_a^2 \int \mathbf{E} \cdot \mathbf{E}_a dv \\ &= -\frac{1}{c} \frac{d}{dt} \left[\frac{4\pi}{c} \int \mathbf{j} \cdot \mathbf{E}_a dv - \int_{S'} (\mathbf{n} \times \mathbf{H}) \cdot \mathbf{E}_a da \right] \\ & \quad - k_a \int_S (\mathbf{n} \times \mathbf{E}) \cdot \mathbf{H}_a da, \end{aligned} \quad (\text{A7a})$$

$$\begin{aligned} & \frac{1}{c^2} \frac{d^2}{dt^2} \int \mathbf{H} \cdot \mathbf{H}_a dv + k_a^2 \int \mathbf{H} \cdot \mathbf{H}_a dv \\ &= k_a \left[\frac{4\pi}{c} \int \mathbf{j} \cdot \mathbf{E}_a dv - \int_{S'} (\mathbf{n} \times \mathbf{H}) \cdot \mathbf{E}_a da \right] \\ & \quad - \frac{1}{c} \frac{d}{dt} \int_S (\mathbf{n} \times \mathbf{E}) \cdot \mathbf{H}_a da. \end{aligned} \quad (\text{A7b})$$

These are the key equations for the EM fields in a hollow cavity. We also obtain the continuity equation from Eqs. (A6c) and (A6d).

First consider an ideal resonant cavity without damping, and assume that the current density is zero in the cavity. Then, the right-hand sides of Eq. (A7) are zero, since \mathbf{E} and \mathbf{H} satisfy $\mathbf{n} \times \mathbf{E} = \mathbf{0}$ on S and $\mathbf{n} \times \mathbf{H} = \mathbf{0}$ on S' as well as \mathbf{E}_a and \mathbf{H}_a in Eq. (A4), respectively. Therefore, the solutions for Eq. (A7) are given by

$$\int \mathbf{E} \cdot \mathbf{E}_a dv = C e^{-i\omega_a t}, \quad (\text{A8a})$$

$$\omega_a = k_a c, \quad (\text{A8b})$$

where C and C' are constants. We also obtain $\int \mathbf{E} \cdot \mathbf{E}_a dv / \int \mathbf{H} \cdot \mathbf{H}_a dv$ from Eq. (A6a) or (A6b) as

$$\frac{\int \mathbf{E} \cdot \mathbf{E}_a dv}{\int \mathbf{H} \cdot \mathbf{H}_a dv} = i. \quad (\text{A9})$$

Thus, ω_a is the angular frequency of a th mode in an ideal resonant cavity with k_a , which is the propagation constant of the a th mode obtained from Eqs. (A3) and (A4).

We next consider a resonant cavity with small damping and assume that $\int \mathbf{E} \cdot \mathbf{E}_a dv$ varies as $e^{-i\omega t}$. Substituting $k_a = \omega_a/c$ into Eq. (A7a) we obtain,

$$\begin{aligned} & \left(\frac{\omega}{\omega_a} - \frac{\omega_a}{\omega} \right) \int \mathbf{E} \cdot \mathbf{E}_a dv \\ &= -i \frac{c}{\omega_a} \left[\frac{4\pi}{c} \int \mathbf{j} \cdot \mathbf{E}_a dv - \int_{S'} (\mathbf{n} \times \mathbf{H}) \cdot \mathbf{E}_a da \right] \\ & \quad + \frac{c}{\omega} \int_S (\mathbf{n} \times \mathbf{E}) \cdot \mathbf{H}_a da. \end{aligned} \quad (\text{A10})$$

Assuming that the form of the complex angular frequency in a resonant cavity with small damping to be $\omega = \omega_a + \Delta\omega_a - i(\omega_a/2Q)$ in the limit of $Q \gg 1$ and $\omega_a \gg \Delta\omega_a$, we then obtain

$$\left(\frac{\omega}{\omega_a} - \frac{\omega_a}{\omega} \right) = 2 \frac{\Delta\omega_a}{\omega_a} - \frac{i}{Q}, \quad (\text{A11})$$

where Q and $\Delta\omega_a$ are the quality factor and the frequency shift from an ideal cavity [27]. Substituting Eq. (A11) into Eq. (A10), and replacing ω to ω_a in the right-hand side of Eq. (A10), we obtain Eq. (9).

Appendix B: Perturbative correction to δf and Q near T_c

To derive expression for the frequency shift very near T_c we carry out a perturbative expansion of Eq. (3) for $\sigma(\omega)$ to second order in $\Delta(T)$,

$$\begin{aligned} \sigma &= \sigma_n + \frac{\sigma_D}{i\omega\tau} \int_{-\infty}^{\infty} \frac{d\epsilon}{4\pi i} \left\{ \tanh\left(\frac{\epsilon - \omega/2}{2T}\right) \frac{\pi}{-2i(\epsilon + i\eta) + 1/\tau} \right. \\ & \quad \times \left[\frac{\Delta^2}{(\epsilon + \omega/2 + i\eta)(\epsilon - \omega/2 + i\eta)} + \frac{\Delta^2}{2(\epsilon - \omega/2 + i\eta)^2} + \frac{\Delta^2}{2(\epsilon + \omega/2 + i\eta)^2} \right] \\ & \quad - \tanh\left(\frac{\epsilon + \omega/2}{2T}\right) \frac{\pi}{2i(\epsilon - i\eta) + 1/\tau} \\ & \quad \times \left[\frac{\Delta^2}{(\epsilon + \omega/2 - i\eta)(\epsilon - \omega/2 - i\eta)} + \frac{\Delta^2}{2(\epsilon - \omega/2 - i\eta)^2} + \frac{\Delta^2}{2(\epsilon + \omega/2 - i\eta)^2} \right] \\ & \quad + \left[\tanh\left(\frac{\epsilon - \omega/2}{2T}\right) - \tanh\left(\frac{\epsilon + \omega/2}{2T}\right) \right] \frac{\pi}{-i\omega + 1/\tau} \\ & \quad \times \left[\frac{\Delta^2}{(\epsilon + \omega/2 + i\eta)(\epsilon - \omega/2 - i\eta)} + \frac{\Delta^2}{2(\epsilon - \omega/2 - i\eta)^2} + \frac{\Delta^2}{2(\epsilon + \omega/2 + i\eta)^2} \right] \left. \right\}. \end{aligned} \quad (\text{B1})$$

Performing the energy integral using the residue theorem choosing integration paths such that the integrands are analytic, and replacing T with T_c except in Δ , we obtain the real and imaginary parts of conductivity as $\sigma_1 = \sigma_{1n} + \sigma_1^{(2)}$ and $\sigma_2 = \sigma_{2n} + \sigma_2^{(2)}$,

with

$$\begin{aligned} \sigma_1^{(2)} = & -2\pi T_c \frac{\sigma_D}{\tau} \Delta^2 \sum_{n=0}^{\infty} \left\{ \frac{2\epsilon_n + 1/\tau}{(2\epsilon_n + 1/\tau)^2 + \omega^2} \left[\frac{1}{\epsilon_n(\epsilon_n^2 + \omega^2)} + \frac{\epsilon_n}{(\epsilon_n^2 + \omega^2)^2} \right] \right. \\ & + \frac{1}{(2\epsilon_n + 1/\tau)^2 + \omega^2} \left[\frac{1}{\epsilon_n^2 + \omega^2} + \frac{\epsilon_n^2 - \omega^2}{2(\epsilon_n^2 + \omega^2)^2} + \frac{1}{2\epsilon_n^2} \right] \\ & + \frac{1/\tau}{1/\tau^2 + \omega^2} \left[\frac{1}{\epsilon_n(\epsilon_n^2 + \omega^2)} + \frac{\epsilon_n}{(\epsilon_n^2 + \omega^2)^2} \right] \\ & \left. + \frac{1}{1/\tau^2 + \omega^2} \left[\frac{1}{\epsilon_n^2 + \omega^2} + \frac{\epsilon_n^2 - \omega^2}{2(\epsilon_n^2 + \omega^2)^2} - \frac{1}{2\epsilon_n^2} \right] \right\}, \end{aligned} \quad (\text{B2})$$

$$\begin{aligned} \sigma_2^{(2)} = & \frac{2\pi T_c}{\omega} \frac{\sigma_D}{\tau} \Delta^2 \sum_{n=0}^{\infty} \left\{ \frac{2\epsilon_n + 1/\tau}{(2\epsilon_n + 1/\tau)^2 + \omega^2} \left[\frac{1}{\epsilon_n^2 + \omega^2} + \frac{\epsilon_n^2 - \omega^2}{2(\epsilon_n^2 + \omega^2)^2} + \frac{1}{2\epsilon_n^2} \right] \right. \\ & - \frac{\omega^2}{(2\epsilon_n + 1/\tau)^2 + \omega^2} \left[\frac{1}{\epsilon_n(\epsilon_n^2 + \omega^2)} + \frac{\epsilon_n}{(\epsilon_n^2 + \omega^2)^2} \right] \\ & + \frac{1/\tau}{1/\tau^2 + \omega^2} \left[\frac{1}{\epsilon_n^2 + \omega^2} + \frac{\epsilon_n^2 - \omega^2}{2(\epsilon_n^2 + \omega^2)^2} - \frac{1}{2\epsilon_n^2} \right] \\ & \left. - \frac{\omega^2}{1/\tau^2 + \omega^2} \left[\frac{1}{\epsilon_n(\epsilon_n^2 + \omega^2)} + \frac{\epsilon_n}{(\epsilon_n^2 + \omega^2)^2} \right] \right\}, \end{aligned} \quad (\text{B3})$$

where $\epsilon_n = (2n + 1)\pi T_c$ is the Matsubara energy at $T = T_c$. Using Eqs. (6) and (B3), and $\sigma_{2n} \approx 0$, the surface resistance and reactance to the second order in Δ are given by

$$\frac{R_s}{R_n} = 1 - \frac{\sigma_1^{(2)} + \sigma_2^{(2)}}{2\sigma_{1n}}, \quad (\text{B4a})$$

$$\frac{X_s}{R_n} = 1 - \frac{\sigma_1^{(2)} - \sigma_2^{(2)}}{2\sigma_{1n}}. \quad (\text{B4b})$$

We finally obtain the frequency shift and quality factor very near T_c from Eqs. (12), (13) and (B4)

$$\delta f = \frac{fR_n}{4G} \frac{\sigma_1^{(2)} - \sigma_2^{(2)}}{\sigma_{1n}}, \quad (\text{B5a})$$

$$Q = \frac{G}{R_n} + \frac{G}{2R_n} \frac{\sigma_1^{(2)} + \sigma_2^{(2)}}{\sigma_{1n}}. \quad (\text{B5b})$$

Thus, as seen in Eq. (B5a), we find an anomaly where the frequency shift is negative in a superconductor near T_c when $\sigma_2^{(2)}$ is larger than $\sigma_1^{(2)}$.

Appendix C: Inhomogenous Disorder

We assume that T_c is Gaussian distributed, and we replace Δ_0 with $\Delta_0 = \pi e^{-\gamma} T_c^{\text{av}}$, where T_c^{av} is the average value of T_c for the cavity. The distribution of T_c is then given by

$$\rho(T_c) = \frac{1}{\sqrt{2\pi\mu_2}} e^{-\frac{(T_c - \mu)^2}{2\mu_2}}, \quad (\text{C1})$$

where μ and $\sqrt{\mu_2}$ are the average and variance, respectively.

We interpret the spread in T_c in terms of inhomogeneity of the disorder, i.e. $1/\tau$. Thus, we infer the probability distribution function for the scattering rate from the Gaussian distribution from the transition temperature. We obtain the probability distribution for $1/\tau$ from Eq.(C1) and the normalization condition,

$$\int_{-\infty}^{\infty} dT_c \rho(T_c) = \int_{-\infty}^{\infty} d\left(\frac{1}{\tau}\right) \tilde{\rho}(1/\tau) = 1, \quad (\text{C2})$$

as

$$\tilde{\rho}(1/\tau) = -\frac{dT_c(1/\tau)}{d(1/\tau)} \frac{1}{\sqrt{2\pi\mu_2}} e^{-\frac{[T_c(1/\tau) - \mu]^2}{2\mu_2}}. \quad (\text{C3})$$

Note that μ and μ_2 are the same as those in Eq. (C1). Function $T_c(1/\tau)$ is calculated by solving Eq. (15), and $dT_c(1/\tau)/d(1/\tau)$ is obtained by differentiating Eq. (15) to obtain,

$$\begin{aligned} \frac{dT_c(1/\tau)}{d(1/\tau)} = & -\frac{T_c}{1/\tau} \\ & \times \frac{\frac{\mathcal{A}}{2} \frac{1/\tau}{2\pi T_{c0}} \sum_{n=0}^{\infty} \frac{1}{\left(n + \frac{1}{2} + \frac{1}{2} \frac{1/\tau}{2\pi T_c}\right)^2}}{\frac{T_c}{T_{c0}} - \frac{\mathcal{A}}{2} \frac{1/\tau}{2\pi T_{c0}} \sum_{n=0}^{\infty} \frac{1}{\left(n + \frac{1}{2} + \frac{1}{2} \frac{1/\tau}{2\pi T_c}\right)^2}}. \end{aligned} \quad (\text{C4})$$

Figure 6 shows the temperature dependence of the disorder-averaged gap near T_c , Gaussian distributions of T_c , and probability distribution function of $1/\tau$ for the four N-doped Nb SRF cavities.

[1] A. Grassellino, A. Romanenko, and Y. Trenikhina et al., *Unprecedented quality factors at accelerating gradients up to 45 MVm⁻¹ in niobium superconducting resonators via low temperature nitrogen infusion*, Supercond. Sci. Tech. **30**, 094004

(2017).
[2] Z. Bogorad, A. Hook, Y. Kahn, and Y. Soreq, *Probing Axion-like Particles and the Axiverse with Superconducting Radio-Frequency Cavities*, Phys. Rev. Lett. **123**, 021801 (2019).

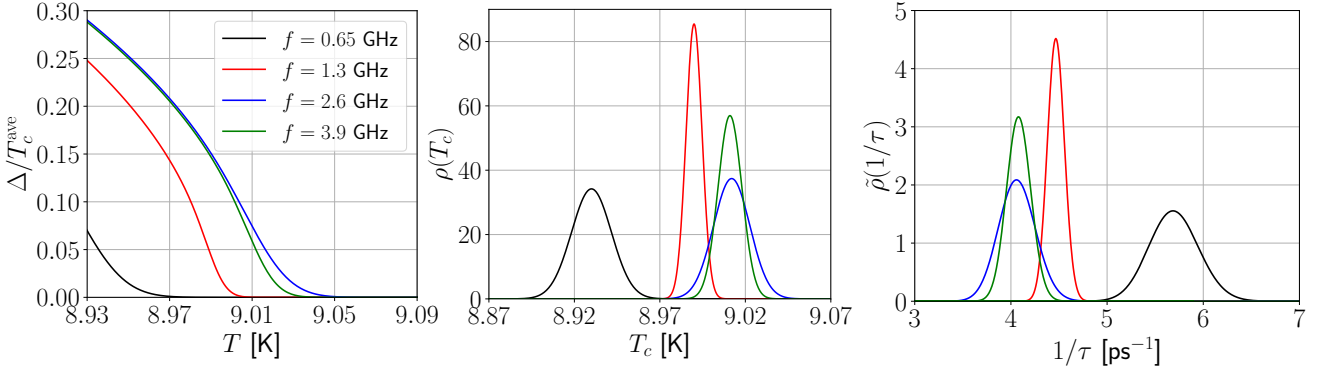


FIG. 6. Gap energy Δ near T_c (left), Gaussian distributions of the transition temperature $\rho(T_c)$ (center), and probability density functions of the relaxation time inverse $\tilde{\rho}(1/\tau)$ (right), for the Nb SRF cavities with each different resonance frequency, $f = 0.65$ GHz (black), 1.3 GHz (red), 2.6 GHz (blue), and 3.9 GHz (green).

- [3] C. Gao and R. Harnik, *Axion searches with two superconducting radio-frequency cavities*, J. High Energ. Phys. **2021**, 53 (2021).
- [4] A. Romanenko, R. Pilipenko, S. Zorzetti, D. Frolov, M. Awida, S. Belomestnykh, S. Posen, and A. Grassellino, *Three-Dimensional Superconducting Resonators at $T < 20$ mK with Photon Lifetimes up to $T_1 = 2$ s*, Phys. Rev. Applied **13**, 034032 (2020).
- [5] A. Gurevich and T. Kubo, *Surface impedance and optimum surface resistance of a superconductor with an imperfect surface*, Phys. Rev. B **96**, 184515 (2017).
- [6] V. Ngampruetikorn and J. A. Sauls, *The Effect of Inhomogeneous Surface Disorder on the Superheating Field of Superconducting RF Cavities*, Phys. Rev. Res. **1**, 012015(R) (2019).
- [7] D. Bafia, A. Grassellino, M. Checchin, J. Zasadzinski, and A. Romanenko, *The Anomalous Resonant Frequency Variation of Microwave Superconducting Niobium Cavities Near T_c* , arXiv **2103.10601** (2021), 10.48550/arXiv.2103.10601.
- [8] C. Varmazis and M. Strongin, *Inductive transition of niobium and tantalum in the 10-MHz range. I. Zero-field superconducting penetration depth*, Phys. Rev. B **10**, 1885 (1974).
- [9] C. Varmazis, J. R. Hook, D. J. Sandiford, and M. Strongin, *Inductive transition of niobium and tantalum in the 10-MHz range. II. The peak in the inductive skin depth for T just less than T_c* , Phys. Rev. B **11**, 3354 (1975).
- [10] O. Klein, E. J. Nicol, K. Holczer, and G. Grüner, *Conductivity coherence factors in the conventional superconductors Nb and Pb*, Phys. Rev. B **50**, 6307 (1994).
- [11] D. Bafia, M. Checchin, A. Grassellino, O. S. Melnychuk, A. S. Romanenko, D. A. Sergatskov, and J. Zasadzinski, *Investigation of Frequency Behavior Near T_c of Niobium Superconducting Radio-Frequency Cavities* (JACoW Publishing, Geneva, Switzerland, 2019) pp. 112–117.
- [12] A. I. Larkin and Y. N. Ovchinnikov, *Quasiclassical Method in the Theory of Superconductivity*, Sov. Phys. JETP **28**, 1200 (1969).
- [13] G. M. Eliashberg, *Inelastic electron collisions and nonequilibrium stationary states in superconductors*, Sov. Phys. JETP **34**, 668 (1972).
- [14] D. Rainer and J. A. Sauls, *Strong-Coupling Theory of Superconductivity*, in *Superconductivity: From Basic Physics to New Developments*, Vol. 1809.05264 (2018) pp. 1–24, published in “Superconductivity: From Basic Physics to New Developments”, ch. 2, pp. 45–78, World Scientific, Singapore (1994).
- [15] J. C. Slater, *Microwave Electronics*, Rev. Mod. Phys. **18**, 441 (1946).
- [16] We set $k_B = \hbar = 1$, in which case $1/\tau$, T_c and ω and Δ have the same units. To convert to Gaussian units: $1/\tau T_c \rightarrow \hbar/\tau k_B T_c$, or $\omega \rightarrow \hbar\omega$, and use Gaussian units for k_B and \hbar .
- [17] M. Zarea, H. Ueki, and J. A. Sauls, *Effects of Anisotropy and Disorder on the Superconducting Properties of Niobium*, Frontiers in Physics **11**, 1269872 (2023).
- [18] A. Gurevich, *Theory of RF superconductivity for resonant cavities*, Supercond. Sci. Technol. **30**, 034004 (2017).
- [19] R. Prozorov, M. Zarea, and J. Sauls, *Niobium in the Clean Limit: an Intrinsic Type I Superconductor*, arXiv: **2207.11829**, 1 (2022).
- [20] B. W. Maxfield and W. L. McLean, *Superconducting Penetration Depth of Niobium*, Phys. Rev. **139**, A1515 (1965).
- [21] C. Benvenuti, S. Calatroni, I. E. Campisi, P. Darrilat, M. A. Peck, R. Russo, and A. M. Valente, *Study of the surface resistance of superconducting niobium films at 1.5 GHz*, Physica C: Superconductivity **316**, 153 (1999).
- [22] D. C. Mattis and J. Bardeen, *Theory of the Anomalous Skin Effect in Normal and Superconducting Metals*, Phys. Rev. **111**, 412 (1958).
- [23] The dimensionless scattering rate can be expressed in terms of other known or measured parameters: $\tau T_{c0} \rightarrow \tau k_B T_{c0}/\hbar = (\ell/\xi_0)/2\pi$, where $\ell = v_f \tau$ is the elastic mean free path in the normal metal, and $\xi_0 = \hbar v_f / 2\pi k_B T_{c0}$ is the superconducting coherence length in the clean limit. Thus, $\tau T_{c0} = 0.1$ corresponds to $\ell/\xi_0 = 0.63$.
- [24] Cavities with other surface treatments also show frequency shift anomalies near T_c , albeit over much wider temperature ranges [c.f. Ref. [28]].
- [25] D. Bafia, Private communication.
- [26] According to Ref. 25 the temperature was measured at the equator, the upper beam pipe, and the lower beam pipe of each cavity using several Cernox RTD temperature sensors, with an observed spread in T_c for each cavity [25].
- [27] J. D. Jackson, *Classical Electrodynamics* (Wiley, New York, 1998).
- [28] H. Ito, High-Q performance of SRF cavities by mid-T baking at KEK, in *Proceedings TESLA Technology Collaboration Meeting 2021* (2021).